Applied Thermal Engineering 233 (2023) 121169

Contents lists available at ScienceDirect

Applied Thermal Engineering

journal homepage: www.elsevier.com/locate/apthermeng

Research Paper

Efficient optimization of parallel micro-channel heat sinks based on flow resistance network model

Lingfeng Yu [a], Jiajun Zhang [a], Xiaoling Wu [b], Jianming Huang [c], Limin Hu [c], Lei Shi [d], Yuan Dong [e,*], Kai Chen [a,*], Bingyang Cao [f,*]

[a] Key Laboratory of Enhanced Heat Transfer and Energy Conservation of the Ministry of Education, School of Chemistry and Chemical Engineering, South China University of Technology, Guangzhou 510640, Guangdong, China
[b] Lab of Applied Biocatalysis, School of Food Science and Engineering, South China University of Technology, Guangzhou 510640, Guangdong, China
[c] Hangzhou Hpwinner Opto Corporation, No. 18 Kangzhou Road, Hangzhou 310015, China
[d] Hangzhou Zhongneng Photoelectric Technology Co. Ltd., Hangzhou 310018, China
[e] School of Mechanical Engineering, Hangzhou Dianzi University, Hangzhou 310018, China
[f] Key Laboratory for Thermal Science and Power Engineering of Ministry of Education, Department of Engineering Mechanics, Tsinghua University, Beijing 100084, China

ARTICLE INFO

Keywords:
Electronics cooling
Micro-channel heat sink
Flow resistance network model
Structural optimization

ABSTRACT

Electronics cooling is a critical issue affecting technological development. Parallel micro-channel heat sink (PMCHS) is widely applied for electronics cooling. However, the existing optimization methods are incapable to perform efficient design of three-dimensional liquid-cooled PMCHSs, impeding the thermal management of high power and volume-shrinking electronics. In this study, a flow resistance network (FRN) model is developed for structural optimization of three-dimensional liquid-cooled PMCHSs. Based on the uniform flow rate distribution, the FRN model is used to determine the optimized parallel channel widths and the optimized inlet deflector shape of the PMCHS. With the optimized parallel channel widths, the maximum temperature (T_{max}) of the PMCHS is decreased by 4.0 K and the temperature standard deviation (σ_T) is decreased by 20%. With the optimized inlet deflector shape, T_{max} and σ_T are reduced by 4.8 K and 14% respectively. The optimization method based on the developed FRN model for structural design of PMCHSs avoids multiple iterations of system parameters in existing optimization methods, showing its potential in high efficient thermal management of electronics.

1. Introduction

As the informatics occupies the frontier of technology industry, the highly reliable and efficient thermal management technology for electronics cooling is on the hotspot. The demand spans from the efficient cooling of data center [1], the cooling of high power insulated gate bipolar transistor (IGBT) [2], the cooling of inverters for solar and wind energy [3], to the battery system of electric vehicles [4].

Large-scale integration of electronics in recent years has enabled the further miniature of electronic equipment with concomitant increase of heat flux, which leads to high hot spot temperature and deteriorates the stability and service life of the electronics [5]. The appropriate operating temperature for electronics, such as chips, ranges from 85 °C to 100 °C. And 1 °C increase in temperature leads to 5% decrease of reliability [6]. Therefore, a cooling system reducing hot spot temperature is desired by the electronics industry. Various kinds of cooling technologies have been developed, including air cooling [7], liquid cooling [8], phase change cooling [9], thermoelectric cooling [10], spray cooling and jet impingement cooling [11]. Among them, liquid cooling technology with micro-channel heat sink (MCHS) is widely used due to its simple and compact structure, as well as high cooling efficiency.

In the existing studies, different MCHSs have been adopted, including serpentine MCHSs [12], tree-like MCHSs [13], rectangle column fin MCHSs [14], and parallel MCHSs [15]. For serpentine micro-channel heat sinks, large local pressure loss exists when the flow direction changes, and the temperature of the cooling liquid downstream is much higher than that upstream as the fluid absorbs the heat when going through the channel, leading to poor temperature uniformity. Though tree-like and rectangle column fin microchannel heat sinks can effectively improve the temperature uniformity, the structure of these systems is complex and high cost. Compared with the other types

* Corresponding authors.
E-mail addresses: dongy@hdu.edu.cn (Y. Dong), chenkaihb09@126.com (K. Chen), caoby@mail.tsinghua.edu.cn (B. Cao).

https://doi.org/10.1016/j.applthermaleng.2023.121169
Received 27 February 2023; Received in revised form 20 May 2023; Accepted 13 July 2023
Available online 17 July 2023

Nomenclature

A	cross-sectional area of the channels, m^2
c_p	specific heat capacity, J/(kg·K)
d	hydraulic diameter of the channels, m
F	a coefficient related to the shape of the channels, 1
H	height of the PMCHS, m
h_C	height of the channels, m
L	length of the PMCHS, m
L_{in}	length of the inlet region of the PMCHS, m
L_{out}	length of the outlet region of the PMCHS, m
l	length of channels, m
$\dot{\mathbf{m}}$	mass flow rate distribution, kg/s
$\dot{m}$	mass flow rate, kg/s
$\dot{m}_0$	inlet mass flow rate of the cooling water, kg/s
$\dot{m}_i$	mass flow rate of the i-th parallel micro-channel, kg/s
N	number of the parallel micro-channels, 1
n	normal vector, 1
P	pressure, Pa
ΔP_{loss}	total pressure loss of the channels, Pa
$\Delta P_{friction}$	pressure loss caused by friction between fluid and channel wall, Pa
ΔP_{local}	pressure loss caused by channel shape, Pa
ΔP	pressure difference, Pa
ΔP_0	pressure loss between the inlet and outlet, Pa
Q_0	inlet volume flow rate of the cooling water, m^3/s
q_0	heat flux exerted on the heating surface, W/m^2
S	area of the heating surface, m^2
T	temperature, K
T_0	inlet temperature, K
U	average velocity of the channel cross section, m/s
u	velocity, m/s
u_0	inlet velocity, m/s
u_i, u_j	i-th and j-th velocity components, m/s
W	width of the PMCHS, m
w_{in}	width of the inlet of the PMCHS, m
w_{out}	width of the outlet of the PMCHS, m
w_T	wall thickness of the PMCHS, m
W_P	power consumption of system, W
$\mathbf{W}$	width distribution, m
w_{PC}	width of the parallel micro-channels, m
w_S	spacing between two adjacent parallel micro-channels, m
$w_{d\text{-}in}$	width of the inlet deflector, m
$w_{d\text{-}out}$	width of the outlet deflector, m
x, y, z	coordinate, m

Greek symbols

ρ	density, kg/m^3
η	dynamic viscosity, kg/(m·s)
λ	thermal conductivity, W/(m·K)
χ	friction coefficient, 1
ξ	local pressure loss coefficient, 1
γ	ratio of flow rate between the branch channel and main channel, 1
Ψ	area ratio between the main channel and the branch channel, 1
$\sigma_{\dot{m}}$	standard deviation of mass flow rate, kg/s
σ_T	standard deviation of temperature, K

Subscripts

avg	average value
f	fluid region
max	maximum value
min	minimum value
opt	optimized system
s	solid region

Acronyms

CC	convergence channel
DC	divergence channel
MCHS	micro-channel heat sink
Nu	Nusselt number
PC	parallel channel
PMCHS	parallel micro-channel heat sink
Re	Reynolds number

of heat sinks, parallel micro-channel heat sinks (PMCHSs) are widely used due to the advantages of simple structure and low pressure loss [16]. However, the structure of parallel channels is easy to induce uneven flow rate distribution among parallel channels, which leads to large temperature difference and high hot spot temperature. Therefore, much efforts have been made to improve the performance of PMCHSs. Xie et al. [17] introduced a series of rectangular-shaped flow obstructions in PMCHSs to enhance their cooling performance. The results showed that the flow obstructions could increase the overall thermal performance by ~1.3 times. Kim et al. [18] used analytical models and numerical method to compare the performance of the PMCHSs with rectangular, inverse trapezoidal, triangular and diamond-shaped cross-sections for micro-channels. They found that the PMCHS with rectangular micro-channels with a high aspect ratio and small fin spacing achieved better thermal performance than those with the other geometries.

Furthermore, optimization algorithms were introduced to design the structure of PMCHSs for improvement of the system performance. Wang et al. [19] combined the CFD method with the simplified conjugate gradient method for optimal geometric design with the minimum overall thermal resistance as the objective. Using this approach, the parameters of channel number, channel aspect ratio and width ratio of channel to pitch were optimized simultaneously. Kumar et al. [16] used combined iterative methods and the computational fluid dynamics (CFD) method to adjust the micro-channel width for homogenization of the flow rates in micro-channels, which reduced the maximum temperature and average temperature by 2.3 °C and 1.1 °C, respectively. Lin et al. [20] adopted a genetic algorithm to optimize the channel number, channel aspect ratio and the ratio of channel width to pitch, with the objectives of minimizing the thermal resistance and weight of the MCHS. The results show that the thermal resistance was decreased by 63% with the weight decreased by 37%. Yildizeli et al. [21] combined elitist NSGA-II and CFD method to optimize the height and width of the micro-channels, and the inlet flow rate, with the target of maximization of Nusselt number and minimization of pump power. Wang et al. [22] set up the baffle structure of cantor fractal in parallel microchannels, and adopted genetic algorithm to optimize the geometry of parallel micro-channels with thermal resistance as the objective function. Kose et al. [23] adopted Non-dominated Sorting Genetic Algorithm II (NSGA-II) to optimize the PMCHSs with three different cross-sections (rectangular, trapezoidal and triangular cross-sections) to increase Nusselt number and reduce pumping power. The study showed that the pumping power of the rectangular micro-channel configuration were 17% and 40% lower than those for trapezoidal and triangular ones, respectively. Shang et al. [24] optimized the PMCHS using NSGA-II, with the objective of reducing thermal resistance and pumping power, finding that the optimized PMCHS reduced the thermal resistance by 25%. Kwanda et al. [25] proposed an improved ε-constraint method combined with surrogated models for optimization of the widths of the micro-channels, the

fin width and depth in a rectangular MCHS to reduce its thermal resistance and pump power. Amador et al. [26] proposed a resistance network model for channel velocity calculation of the microchannel reactor under creeping flow with low Reynolds number. Based on this simplified model, Li et al. [27] calculated the parallel channel widths and outlet manifold structure of micro-channel reactors for equal velocities in parallel channels. In Chen's work [28], a similar flow resistance network (FRN) model was adopted to calculate the flow rate distribution in the parallel air-cooled battery thermal management system, and optimization of parallel channel widths was conducted by adjusting the flow rate distribution and using the FRN model, which reduced the temperature difference of the battery pack by 55%.

Previous studies have showed that structural parameters significantly affect the cooling performance of PMCHSs. Employing optimization methods for structural design has been demonstrated to be effective for improving the PMCHSs performance. The traditional optimization methods in the previous studies, such as iterative method or NSGA-II, usually need repetitive evaluations of system performance and are time-consuming. By comparison, the method based on the FRN model and pre-set optimized velocity distribution is efficient to obtain the optimized structural parameters of parallel channel system. However, the existing FRN models are mainly applicable to the systems with creeping flow or the air-cooled systems, which cannot be directly applied to three-dimensional liquid-cooled PMCHSs. It is highly desirable to develop an effective FRN model for flow rate calculation of three-dimensional PMCHSs and propose the efficient optimization method for structural design of PMCHSs.

In this study, the FRN idea is introduced to design PMCHSs. The FRN model is developed to establish the quantitative relationship between the structural parameters of three-dimensional liquid-cooled PMCHSs and the flow rates in parallel micro-channels. By assuming the equal flow rate distribution, the optimized structural parameters of PMCHSs are calculated directly. The influence of the shape of the inlet and outlet deflectors is investigated. Then the widths of parallel micro-channels and the deflector shape of the PMCHSs are optimized using the FRN model. The comparison of these optimized systems is conducted to verify the effectiveness of the optimization based on FRN model for efficient design of PMCHSs.

2. Model of PMCHS

The scheme of the PMCHS investigated is shown in Fig. 1. One side of the PMCHS is attached to the heat source (named heating surface). The cooling fluid removes the heat from the heat source when going through the PMCHS from the inlet, leading to reduction of the heat source temperature. The PMCHS contains 10 parallel micro-channels with identical width as 1 mm. The spacings between two adjacent parallel micro-channels are equal of 1 mm. The values of other structural parameters of the PMCHS are listed in Table 1. The cooling medium in the PMCHS is water, and the solid part is made of copper. The physical parameters of water and copper are shown in Table 2.

3. Numerical method

3.1. Governing equations and boundary conditions

In this work, computational fluid dynamics (CFD) method is used to calculate the velocity and temperature fields in the three-dimensional PMCHS, to evaluate the performance of the PMCHS. The small channel size in PMCHSs leads to low Reynolds number, suggesting a laminar flow in the system. The governing equations of steady incompressible laminar flow are introduced as follows:

Continuity equation:

$$\frac{\partial u_j}{\partial x_j} = 0 \tag{1}$$

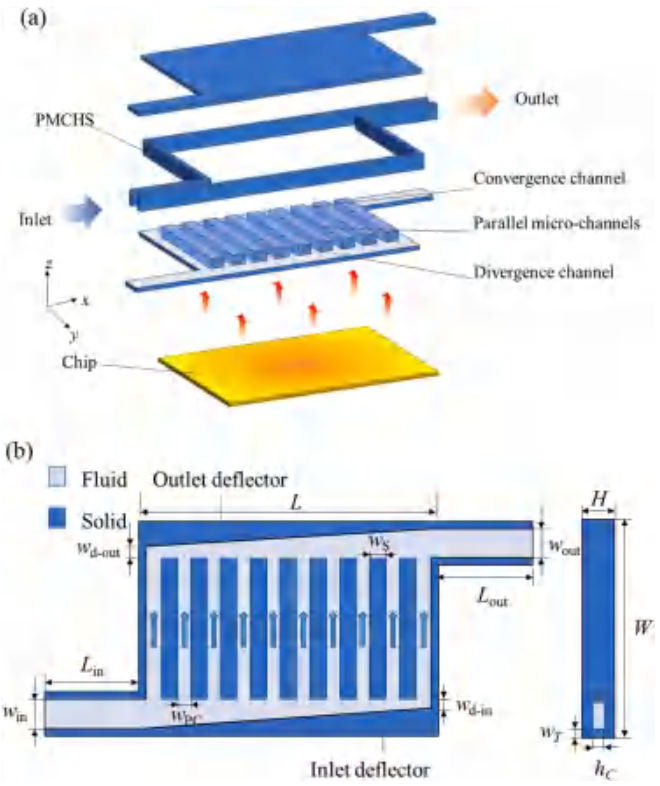

Fig. 1. Schemes of the PMCHS: (a) three-dimensional system, (b) two-dimensional system.

Table 1
The values of other structural parameters of the PMCHS.

Parameters	Values (mm)
Length, width and height (L, W, H)	20, 17, 1.5
Length of the inlet and outlet (L_{in}, L_{out})	7.5, 7.5
Width of the inlet and outlet (w_{in}, w_{out})	3
Wall thickness (w_T)	0.5
Width of the parallel micro-channels (w_{PC})	1
Spacing of the adjacent micro-channels (w_S)	1
Height of the channels (h_C)	0.5

Table 2
The physical parameters of water and copper.

Values	Copper	Water
Density (ρ, kg/m^3)	8930	998.2
Specific heat capacity (c_p, J/(kg·K))	386	4182
Thermal conductivity (λ, W/(m·K))	398	0.6
Dynamic viscosity (η, kg/(m·s))	/	0.001003

Momentum equation:

$$\frac{\partial(\rho_f u_i u_j)}{\partial x_j} = -\frac{\partial P}{\partial x_i} + \frac{\partial}{\partial x_j}\left(\eta_f \frac{\partial u_i}{\partial x_j}\right) \tag{2}$$

where u_i and u_j represent the i-th and j-th velocity components. ρ_f, P and η_f represent the density, pressure and dynamic viscosity coefficient, respectively. The subscripts f represents the variables of the fluid regions.

To calculate the temperature fields of the PMCHS, the energy equations are introduced:

For fluid region:

$$\rho_f c_{P,f} \frac{\partial (u_j T_f)}{\partial x_j} = \frac{\partial}{\partial x_j}\left(\lambda_f \frac{\partial T_f}{\partial x_j}\right) \tag{3}$$

For solid region:

$$\frac{\partial}{\partial x_j}\left(\lambda_s \frac{\partial T_s}{\partial x_j}\right) = 0 \tag{4}$$

where the subscript s represents the variables of the solid regions. T represents the temperature.

In order to solve the above governing equations, the following boundary conditions are adopted: The inlet is set to mass flow inlet with constant temperature, and the outlet is set to pressure outlet. The interfaces between the fluid and solid regions are set to non-slip conditions. Constant heat flux is applied to the heating surface of the PMCHS to simulate chip heating, and the other borders are set to adiabatic conditions. The boundary conditions are listed as follows:

Inlet:

$$u_x = u_0, T_w = T_0 \tag{5}$$

Interfaces of fluid and solid:

$$u = 0 \tag{6}$$

Heating surface:

$$-\lambda_s \frac{\partial T_s}{\partial n} = q_0 \tag{7}$$

Other borders:

$$\frac{\partial T_s}{\partial n} = 0 \tag{8}$$

where q_0 represents the heat flux exerted on the heating surface. u_0 and T_0 represent the inlet velocity and inlet temperature of the water respectively. In this study, T_0 and q_0 are set to 293.15 K and 2×10^5 W/m^2, respectively. The inlet mass flow rate is set to 1 g/s.

3.2. Grid-dependence analysis

The regular shape of the PMCHS implied that using structural grids to divide the computational area for calculation is suitable, as shown in Fig. 2a. With consideration of calculation speed and accuracy, grid-dependence test was conducted to determine the size of the grids. CFD calculations with various grid numbers were conducted, with the results shown in Fig. 2b, where T_{max} and σ_T represent the maximum temperature and temperature standard deviation of the heating surface. When the grid number is small, T_{max} and σ_T increase with larger grids number. When the grid number is greater than 1.08×10^6, the variation of T_{max} and σ_T is less than 0.05 K, which suggests that the results are independent of the grids when the number is 1.08×10^6. Thus, in the subsequent calculation, a grid number of 1.08×10^6 was adopted.

3.3. Validation of the numerical method

To verify the numerical method, the laminar flow in a rectangular channel is introduced, and the numerical results are compared with the analytical one. The rectangular channel with different sizes ($a \times b \times l$) are considered, with the values listed in Table 3. The same cooling water with properties listed in Table 2 is adopted. The inlet Reynolds number (Re) is set to 133. The H1 (axially uniform heat flux and peripherally uniform temperature) thermal boundary conditions are used with the heat flux as 2×10^4 W/m^2. Previous study has derived the analytical results of Nusselt number (Nu) under H1 conditions for the fully developed laminar flow [29]. Table 3 lists the comparison of the numerical and analytical results. We can see that the Nu results by numerical method are consistent with the analytical results under different conditions, with the relative deviation no more than 0.5%. Thus, the accuracy and reliability of the numerical method adopted in this study is verified.

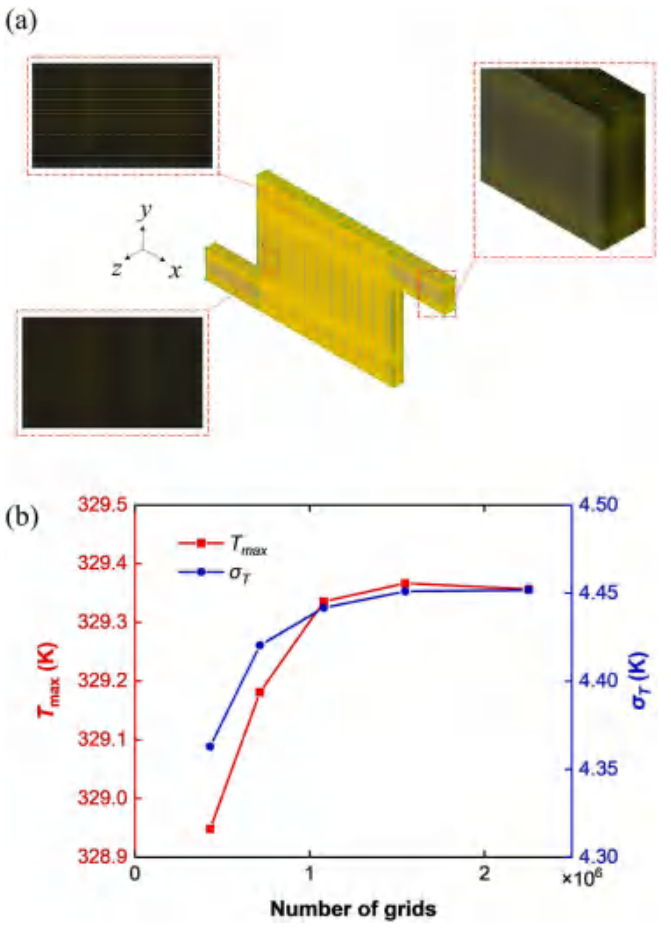

Fig. 2. Grid dependence test: (a) grid system, (b) results of grid dependence test.

Table 3
Comparison of numerical results and analytical results in rectangular channels (Re = 133).

a/b	a (mm)	b (mm)	l (mm)	Nu		Deviation
				Numerical method	Analytical method [29]	
1	0.5	0.5	200	3.60	3.61	0.3%
2	1	0.5	200	4.11	4.12	0.2%
4	2	0.5	200	5.31	5.33	0.4%
8	4	0.5	200	6.46	6.49	0.5%
∞	∞	0.5	200	8.25	8.23	0.2%

4. Flow resistance network model

4.1. Governing equations

The CFD method is effective to evaluate the cooling performance of the PMCHS with high reliability and accuracy. However, this method needs to solve complex differential equations, which costs a large amount of computational time. Liu et al. [30] and Zhang et al. [31] respectively established the flow resistance network (FRN) model to quickly calculate the channel velocities in parallel air-cooled battery thermal management systems with different flow patterns. As the structure of three-dimensional PMCHSs is similar to that of parallel air-cooled systems, the similar FRN model is adopted to accelerate the

calculation of flow rate distribution in PMCHSs. In this model, the pressure loss of the cooling water exerted by the channels is equivalent to flow resistance, and the PMCHS is equivalent to the FRN as shown in Fig. 3, in which each block represents the flow resistance of the corresponding channel segment. In Fig. 3, DC, PC and CC represent the divergence channel, parallel micro-channels, and convergence channel, respectively. For each loop in the FRN, the following pressure loss equation is satisfied [30].

$$\Delta P_{\mathrm{loss,DC},i+1} + \Delta P_{\mathrm{loss,PC},i+1} - \Delta P_{\mathrm{loss,PC},i} - \Delta P_{\mathrm{loss,CC},i} = 0, \quad i = 1, 2, \cdots, N-1 \tag{9}$$

where ΔP_{loss} is the total channel pressure loss, expressed as:

$$\Delta P_{\mathrm{loss}} = \Delta P_{\mathrm{friction}} + \Delta P_{\mathrm{local}} \tag{10}$$

where $\Delta P_{\mathrm{friction}}$ is the frictional loss, which is the pressure loss caused by friction between fluid and channel walls. $\Delta P_{\mathrm{local}}$ is the local loss, which is the loss caused by the channel shape. According to Darcy friction equation, $\Delta P_{\mathrm{friction}}$ can be expressed as follows:

$$\Delta P_{\mathrm{friction,DC},i} = \chi_{\mathrm{DC},i} \frac{l_{\mathrm{DC},i}}{2d_{\mathrm{DC},i}} \rho_{\mathrm{f}} U_{\mathrm{DC},i}^2 \tag{11}$$

$$\Delta P_{\mathrm{friction,CC},i} = \chi_{\mathrm{CC},i} \frac{l_{\mathrm{CC},i}}{2d_{\mathrm{CC},i}} \rho_{\mathrm{f}} U_{\mathrm{CC},i}^2 \tag{12}$$

$$\Delta P_{\mathrm{friction,PC},i} = \chi_{\mathrm{PC},i} \frac{l_{\mathrm{PC},i}}{2d_{\mathrm{PC},i}} \rho_{\mathrm{f}} U_{\mathrm{PC},i}^2 \tag{13}$$

where U is the average velocity in the channels. ρ_{w} is the density of cooling water. l and d are the length and hydraulic diameter of the channels. χ is the friction coefficient, expressed as:

$$\chi = F \frac{64}{Re} \tag{14}$$

where F is a coefficient related to the shape of the channels. Re is the Reynolds number. $\Delta P_{\mathrm{local}}$ can be expressed as:

$$\Delta P_{\mathrm{local,DC},i} = \frac{\xi_{\mathrm{DC},i}}{2} \rho_{\mathrm{f}} U_{\mathrm{DC},i}^2 \tag{15}$$

$$\Delta P_{\mathrm{local,CC},i} = \frac{\xi_{\mathrm{CC},i}}{2} \rho_{\mathrm{f}} U_{\mathrm{CC},i}^2 \tag{16}$$

$$\Delta P_{\mathrm{local,PC},i} = \frac{\xi_{\mathrm{CC}\to\mathrm{PC},i}}{2} \rho_{\mathrm{f}} U_{\mathrm{DC},i}^2 + \frac{\xi_{\mathrm{PC}\to\mathrm{CC},i}}{2} \rho_{\mathrm{f}} U_{\mathrm{CC},i}^2 \tag{17}$$

where ξ is the local pressure loss coefficient. Bassett et al. [32] derived the expression of ξ as follows:

$$\xi_{\mathrm{CC},i} = 1 - \gamma_{\mathrm{CC},i}^2 \tag{18}$$

$$\xi_{\mathrm{PC}\to\mathrm{CC},i} = \gamma_{\mathrm{PC}\to\mathrm{CC},i}^2 \Psi_{\mathrm{PC}\to\mathrm{CC},i}^2 + 2\left(2\gamma_{\mathrm{PC}\to\mathrm{CC},i} - \gamma_{\mathrm{PC}\to\mathrm{CC},i}^2\right) - 1 \tag{19}$$

$$\xi_{\mathrm{DC},i} = \gamma_{\mathrm{DC},i}^2 - \frac{3}{2}\gamma_{\mathrm{DC},i} + \frac{1}{2} \tag{20}$$

$$\xi_{\mathrm{DC}\to\mathrm{PC},i} = \gamma_{\mathrm{DC}\to\mathrm{PC},i}^2 \Psi_{\mathrm{DC}\to\mathrm{PC},i}^2 - 2\frac{3\pi}{8}\gamma_{\mathrm{DC}\to\mathrm{PC},i}\Psi_{\mathrm{DC}\to\mathrm{PC},i}^2 + 1 \tag{21}$$

where γ is the ratio of flow rate between the branch channel and main channel. Ψ is the area ratio between the main channel and branch channel.

Moreover, the flow conservation equations are satisfied at the inlet and outlet of the parallel channels which are expressed as follows:

$$\dot{m}_0 = \rho_{\mathrm{f}} U_{\mathrm{DC},1} A_{\mathrm{DC},1} \tag{22}$$

$$\rho_{\mathrm{f}} U_{\mathrm{DC},i} A_{\mathrm{DC},i} = \rho_{\mathrm{f}} U_{\mathrm{DC},i+1} A_{\mathrm{DC},i+1} + \rho_{\mathrm{f}} U_{\mathrm{PC},i} A_{\mathrm{PC},i}, i = 1, 2, \cdots, N-1 \tag{23}$$

$$\rho_{\mathrm{f}} U_{\mathrm{CC},i} A_{\mathrm{CC},i} = \rho_{\mathrm{f}} U_{\mathrm{CC},i-1} A_{\mathrm{CC},i-1} + \rho_{\mathrm{f}} U_{\mathrm{PC},i} A_{\mathrm{PC},i}, i = 1, 2, \cdots, N \tag{24}$$

where $\dot{m}_0$ represents the inlet mass flow rate of the cooling water. A is the cross-sectional area of the channels. N is the number of parallel micro-channels. Eqs. (9)–(24) constitute the governing equations of the FRN model. With the structural parameters and inlet mass flow rate given, the mass flow rate of each channel in PMCHSs can be calculated using the FRN model.

4.2. Validation of the FRN model

In order to verify the effectiveness of the FRN model, the results from the model is compared with those obtained from the CFD method. In order to improve the accuracy of the results from the FRN model, the coefficient related to the channel shape (F) is set to 0.785 for the investigated three-dimensional liquid-cooled PMCHS, which is different from that for the air-cooled system in the previous study [31]. Fig. 4 shows the comparison of the mass flow rates in different channels. It can be seen that the results of the FRN model and the CFD method are in good agreement. The average deviations of the mass flow rates in DCs,

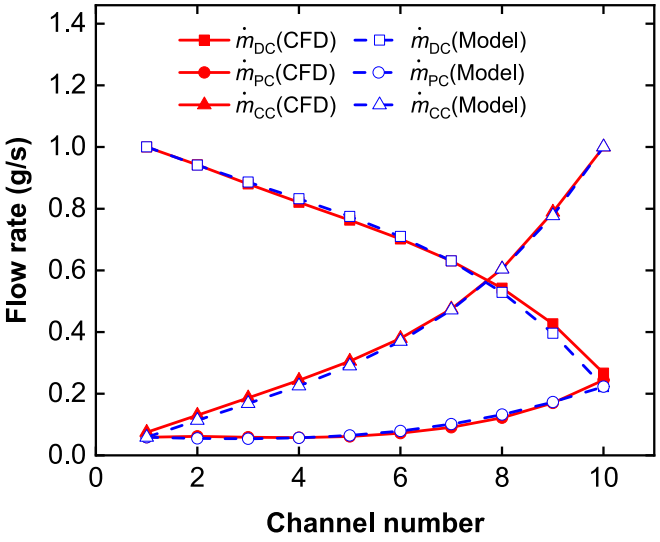

Fig. 4. Comparison of the results of the FRN model and CFD method.

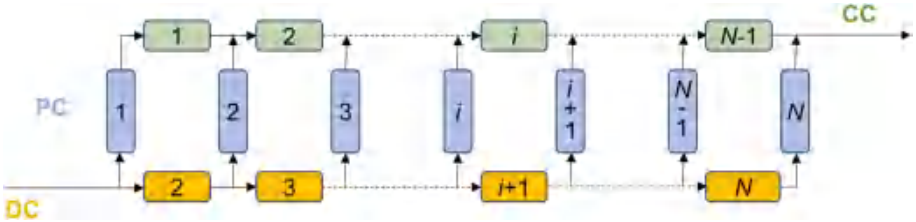

Fig. 3. Schematic diagram of the FRN model.

PCs and CCs are 3%, 6% and 7%, respectively. Compared with several hours of calculation time needed in CFD method, the FRN model only takes seconds to obtain the results with similar accuracy. Therefore, the FRN model can lead us to obtain the mass flow rate distribution in a short time, which can be used to evaluate the performance of PMCHSs and accelerate the structural optimization of system.

5. Optimization of PMCHSs

5.1. Performance of PMCHSs before optimization

The velocity and temperature fields of the PMCHS with identical widths of micro-channels considered in Section 2 (denoted as PMCHS-0) were calculated using the CFD method. The performance of the PMCHS is evaluated by the maximum temperature (T_{max}), standard deviation of the flow rates ($\sigma_{\dot{m}}$) of the micro-channels, standard deviation of the temperature (σ_T) of the heating surface and pumping power of the system (W_P). The expressions of the characteristic parameters are shown as follows:

$$\sigma_{\dot{m}} = \sqrt{\frac{\sum_{i}^{N}\left(\dot{m}_i - \dot{m}_{avg}\right)^2}{N-1}} \tag{25}$$

$$\sigma_T = \sqrt{\frac{\iint_S \left(T - T_{avg}\right)^2 dS}{S}} \tag{26}$$

$$W_P = Q_0 \times \Delta P_0 \tag{27}$$

where $\dot{m}_i$ represents the mass flow rate of the i-th parallel micro-channel, and m_{avg} represents the average flow rate of all channels. T_{avg} is the average temperature of the heating surface, and S represents the area of the heating surface. Q_0 represents the inlet volume flow rate of the cooling water. ΔP_0 represents the pressure loss between the inlet and outlet.

Fig. 5a depicts the flow contour in PMCHS-0, which shows uneven distribution of flow rates among parallel channels. From the inlet to the outlet, the flow rates of parallel channels gradually increase, with the ratio of the maximum to the minimum one as high as 4.15. Thus, the hot spot temperature on the heat surface is located at the downstream of the parallel channels near the inlet (Fig. 6a). It can be observed that T_{max} of the PMCHS reaches 329.3 K, and σ_T is 4.44. The high hot spot temperature and large temperature difference on heat surface of PMCHS-0 result from the large flow rate difference among parallel channels. In this section, based on the FRN model, the structure of the PMCHS is first optimized to homogenize the flow rate distribution in parallel channels, which is expected to improve the cooling performance of the PMCHS.

5.2. Optimization of parallel micro-channel widths

The quantitative relationship between the structural parameters of PMCHSs and the flow rates in channels has been built up based on the FRN model. Once the inlet flow rate and the structural parameters of the system are given, the flow rates in parallel channels can be obtained by solving the FRN model. Conversely, the structural parameters can be calculated by solving the model if the flow rates in parallel channels are given [33]. Therefore, with the assistance of the FRN model, the structural optimization problem of PMCHSs is transformed into a simpler one that searches the optimal flow rate distribution among parallel channels. The analysis in Section 5.1 has revealed that reducing the flow rate difference in parallel channels is conducive to the improvement of the cooling performance in PMCHSs. Therefore, in this section, based on the FRN model, the widths of parallel micro-channels in the PMCHS are optimized to homogenize the flow rate distribution for improvement of the PMCHS performance. For convenience, the width distribution of parallel channels and corresponding flow rate distribution are defined as $\mathbf{W_{PC}}$ and $\dot{\mathbf{m}}_{PC}$ respectively, expressed as follows:

$$\mathbf{W_{PC}} = \left[w_{PC,1}, \cdots, w_{PC,i}, \cdots, w_{PC,N}\right] \tag{28}$$

$$\dot{\mathbf{m}}_{PC} = \left[\dot{m}_{PC,1}, \cdots, \dot{m}_{PC,i}, \cdots, \dot{m}_{PC,N}\right] \tag{29}$$

where $w_{PC,i}$ and $\dot{m}_{PC,i}$ represent the width and corresponding flow rate of the i-th parallel channel. When optimizing $\mathbf{W_{PC}}$, it is assumed that $\dot{\mathbf{m}}_{PC}$ is uniformly distributed, and the unknown variables are $U_{PC,i}$, $U_{CC,i}$, $U_{DC,i}$ and $w_{PC,i}$, with a total number of 4 N. The FRN model Eqs. (9) and (22)–(24) give (4 N−1) equations. To solve the unknown variables, an equation which guarantees the sum of parallel channel widths is a constant is added, expressed as:

$$\sum_{i=1}^{N} w_{PC,i} = \text{const} \tag{30}$$

Thus, when the optimal $\dot{\mathbf{m}}_{PC}$ is given, the optimized widths of parallel channels can be calculated by solving Eqs. (9), (22)–(24) and (30).

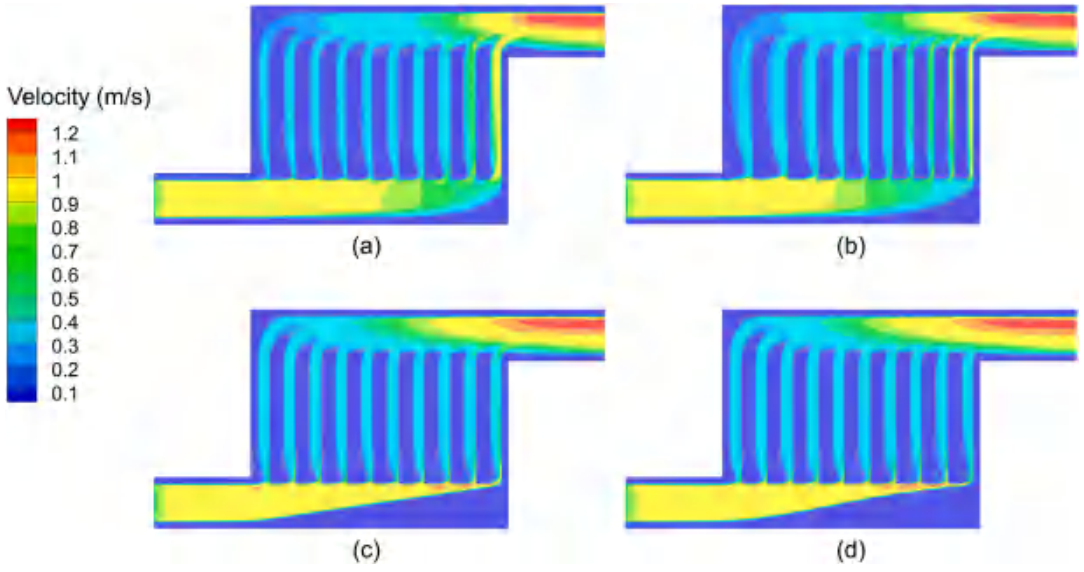

Fig. 5. Flow contours of different PMCHSs: (a) PMCHS-0, (b) PMCHS-opt1, (c) PMCHS-opt2, (d) PMCHS-opt3.

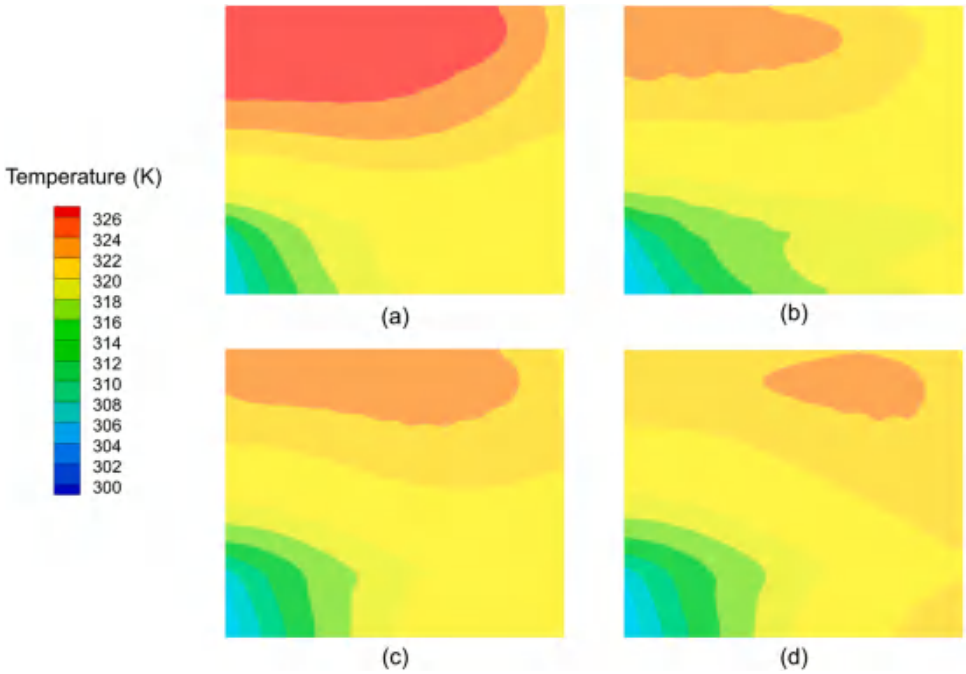

Fig. 6. Temperature contours of different PMCHSs: (a) PMCHS-0, (b) PMCHS-opt1, (c) PMCHS-opt2, (d) PMCHS-opt3.

Considering the PMCHS in Section 2, the inlet flow rate $\dot{m}_0$ is set to 1 g/s. The total width of the parallel channels is 10 mm, and the number of parallel channels is 10. The optimal flow rate distribution $\dot{\mathbf{m}}_{PC}$ is set to a uniform distribution. By using the FRN model, the optimized width distribution $\mathbf{W}_{PC,opt}$ is calculated, with the results shown in Eq. (31).

$$\mathbf{W}_{PC,opt} = [1.88,\ 1.71,\ 1.36,\ 1.08,\ 0.89,\ 0.77,\ 0.67,\ 0.6,\ 0.54,\ 0.5]\ \text{mm} \tag{31}$$

The cooling performance of the PMCHS with the optimized parallel channel widths (denoted as PMCHS-opt1) is evaluated using the CFD method, and is compared with that of PMCHS-0 before optimization. Fig. 5b shows the flow contour of PMCHS-opt1. It can be seen from $\mathbf{W}_{PC,opt}$ and Fig. 5b that, from the inlet to outlet, the optimized channel width gradually decreases in the order. When the channel width increases, the drag of water exerted by the chancel walls decreases, leading to more water going through the channels. For PMCHS-0, the flow rates of parallel channels are increased in the order of position from the inlet to the outlet (Fig. 7). After the optimization of micro-channel widths, the wider channel near the inlet leads to the increase of the corresponding flow rates, and the narrower channel near the outlet decreases the corresponding flow rates. Therefore, the gradually narrower channel from the inlet to the outlet after optimization is effective for homogenization of the flow rate distribution of parallel channels, which ensured the reduced hot spot temperature and resultant improved temperature uniformity of the heating surface.

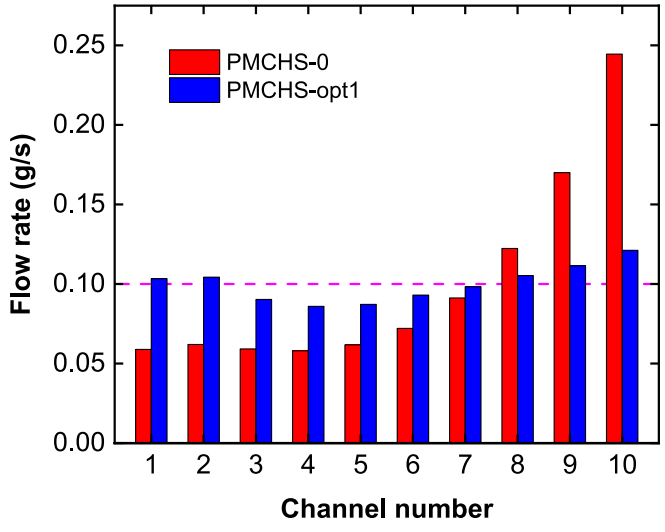

Fig. 7. Flow rates of parallel channels in PMCHSs before and after optimization of channel widths.

It can be seen from Fig. 7 that the flow rates of parallel channels in PMCHS-opt1 are all around 0.1 g/s, which are similar to the pre-set uniform flow rate distribution. The average deviation of the flow rate distribution in PMCHS-opt1 and the pre-set uniform one is only 6%, which verifies the accuracy of the FRN model for the PMCHS with uneven micro-channel widths. The results demonstrate that the parallel channel width distribution corresponding to the given flow rate distribution can be effectively calculated by the FRN model. Compared with PMCHS-0, the uniformity of the flow rates in parallel channels in PMCHS-opt1 is greatly improved, with $\sigma_{\dot{m}}$ at 0.011 g/s, which is reduced by 82%. The significant reduction of flow rate difference ensured the effective improvement of cooling performance of the PMCHS. Fig. 6b shows the temperature contour of the heating surface in PMCHS-opt1. We can observe that the hot spot temperature is still located at the downstream of the channels close to the inlet for PMCHS-opt1, but is much lower than that in PMCHS-0, as the mass flow rate at this micro-channel is increased by 75% after the channel width optimization (Fig. 7). T_{max} and σ_T in PMCHS-opt1 respectively decrease by 4.0 K and 20% compared with those in PMCHS-0 (Table 4). Moreover, the pumping power of the PMCHS does not increase after the micro-channel width optimization. Thus, optimizing the parallel micro-channel widths

Table 4
Comparison of the performance of different PMCHSs ($\dot{m}_0$=1 g/s).

PMCHS	$\sigma_{\dot{m}}$(g/s)	T_{max} (K)	σ_T (K)	W_P (W)
0	0.0625	329.3	4.44	0.00101
opt1	0.0113	325.3	3.57	0.00105
opt2	0.0096	324.8	3.74	0.00123
opt3	0.0079	324.5	3.81	0.00125

by using the FRN model can significantly improve the cooling performance of PMCHSs without increasing the pumping power.

5.3. Optimization of deflector shape

In addition to the parallel channel widths, the shape of the inlet and outlet deflectors significantly affects the flow rate distribution in parallel channels. Therefore, in this section, the shape of the deflectors is designed to homogenize the flow rate distribution in parallel channels for improvement of heat dissipation performance of PMCHSs.

5.3.1. Optimization of the straight-line deflector

In this section, straight-line deflectors are considered, and the flow rate distribution of parallel channels is adjusted by designing the deflector angles. For convenience, the angles of the inlet and outlet deflectors are adjusted by the inlet width ($w_{\text{d-in}}$) and outlet width ($w_{\text{d-out}}$), as shown in Fig. 1. The values of $w_{\text{d-in}}$ and $w_{\text{d-out}}$ are ranging within [0, w_{in}] and [0, w_{out}], respectively.

According to the analysis in Section 5.1, the homogenization of flow rate distribution of parallel channels will improve the cooling performance of PMCHSs. $\sigma_{\dot{m}}$ expressed as Eq. (25) is used to characterize the uniformity of the mass flow rates. Smaller $\sigma_{\dot{m}}$ represents more uniform flow rate distribution. Therefore, in this section, the angles of the inlet and outlet deflectors are optimized with the objective of minimizing $\sigma_{\dot{m}}$. There situations are considered as follows:

Condition 1: Let $w_{\text{d-out}} = w_{\text{out}} = 3$ mm, $w_{\text{d-in}}$ is adjusted within [0, w_{in}].
Condition 2: Let $w_{\text{d-in}} = w_{\text{in}} = 3$ mm, $w_{\text{d-out}}$ is adjusted within [0, w_{out}].
Condition 3: Let $w_{\text{d-in}} = w_{\text{d-out}}$, $w_{\text{d-in}}$ and $w_{\text{d-out}}$ is adjusted within [0, w_{in}].

For each condition, there is only one variable to be optimized, $w_{\text{d-in}}$ or $w_{\text{d-out}}$. Thus, the value of $w_{\text{d-in}}$ or $w_{\text{d-out}}$ is set at the interval of 0.1 mm. The $\sigma_{\dot{m}}$ value for each $w_{\text{d-in}}$ or $w_{\text{d-out}}$ is evaluated using the FRN model. The evaluation results of different conditions are shown in Fig. 8, where the horizontal and vertical coordinates represent the $w_{\text{d-in}}/w_{\text{d-out}}$ value and the corresponding $\sigma_{\dot{m}}$ value. Moreover, $w = 3.0$ mm indicates PMCHS-0. For Condition 1, as can be seen from Fig. 8, with the decrease of $w_{\text{d-in}}$, the inlet deflector angle increases, and $\sigma_{\dot{m}}$ decreases first and then increases. When $w_{\text{d-in}} = 0.2$ mm, $\sigma_{\dot{m}}$ reaches the minimum value. It indicates that the homogenization of the flow rates in parallel channels can be significantly improved by adjusting the inlet deflector angle only. For Condition 2, with the decrease of $w_{\text{d-out}}$, the outlet deflector angle increases and $\sigma_{\dot{m}}$ increases, indicating that increasing the outlet deflector angle worsens the uniformity of flow rates. For Condition 3, as $w_{\text{d-in}}$ and $w_{\text{d-out}}$ decrease, the angles of the inlet and outlet deflectors increases simultaneously, and $\sigma_{\dot{m}}$ decreases first and then increases, which is similar to Condition 1. But the minimum $\sigma_{\dot{m}}$ is larger than that of Condition 1. Therefore, it is better to adjust the inlet deflector angle only and the best $w_{\text{d-in}}$ is 0.2 mm will achieve system with better cooling performance, and the corresponding PMCHS is denoted as PMCHS-opt2.

The CFD method was used to evaluate the performance of PMCHS-opt2, and Fig. 5c shows the flow contour of PMCHS-opt2. As can be seen, after introduction of straight-line deflector at the inlet, the flow rate distribution of parallel channels in PMCHS-opt2 is much more uniform than that in PMCHS-0. Fig. 9 shows the comparison of the flow rate distribution for PMCHS-0 and PMCHS-opt2. It can be observed that the flow rate distribution in PMCHS-opt2 is similar to the set uniform distribution. $\sigma_{\dot{m}}$ of PMCHS-opt2 is 0.0096, which is reduced by 85% compared with that of PMCHS-0. The improvement of the flow rate distribution is attributed to reduction of the pressure loss difference among the parallel channels. Fig. 10 shows the pressure of the inlet and outlet of the parallel channels, and the corresponding pressure loss of each parallel channel in PMCHS-0 and PMCHS-opt2. For PMCHS-0, the pressure loss of the channels increases with the channel number. It means that the pressure loss of the channels far from the inlet is larger than that near the inlet. Larger pressure loss leads to more flow rates in the channel. Thus, the flow rates increase with the channel number for PMCHS-0, as shown in Fig. 9. For PMCHS-opt2, the angle of the inlet deflector increases, and the cross-section area of the divergence channel far from the inlet decreases, which increases the local velocity of the water. According to Bernoulli equation, the local pressure is reduced. Therefore, for PMCHS-opt2, the inlet pressure of the parallel channels far from the inlet decreases, significantly reducing the difference of the pressure loss among parallel channels (Fig. 10b), leading to more uniform flow rate distribution among parallel channels.

The significant reduction of flow rate difference results in effective improvement of the cooling performance of the PMCHS (Table 4). Fig. 6c shows the temperature contour of the heating surface in PMCHS-opt2. We can observe that, similar to PMCHS-0, the hot spot temperature is still located at the downstream of the channels close to the inlet for PMCHS-opt2, but is lower than that in PMCHS-0 as the mass flow rate at this micro-channel is increased by 88% after the optimization of the inlet deflector angle (Fig. 9). $T_{\max}$ of PMCHS-opt2 is only 324.8 K and σ_T is 3.74 K, which are respectively reduced by 4.5 K and 16% compared with

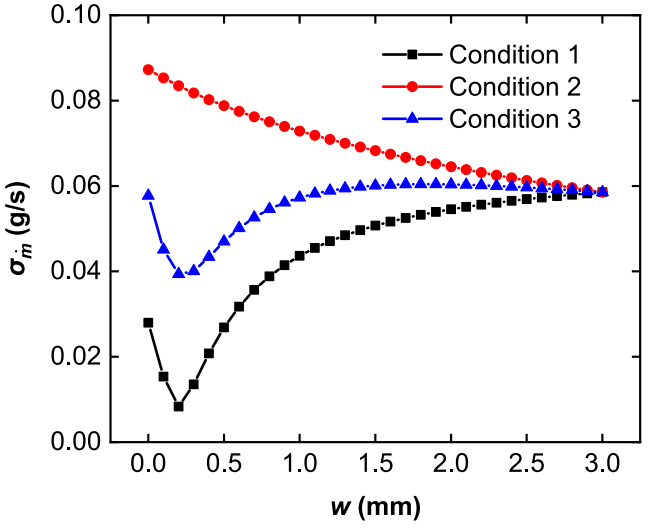

Fig. 8. Standard deviation of the flow rates in parallel channels for different conditions ($\dot{m}_0$=1 g/s).

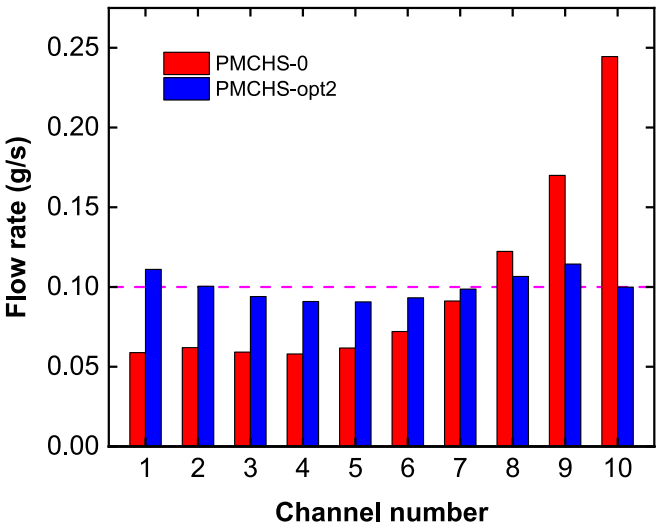

Fig. 9. Flow rates of the parallel channels in PMCHS-0 and PMCHS-opt2.

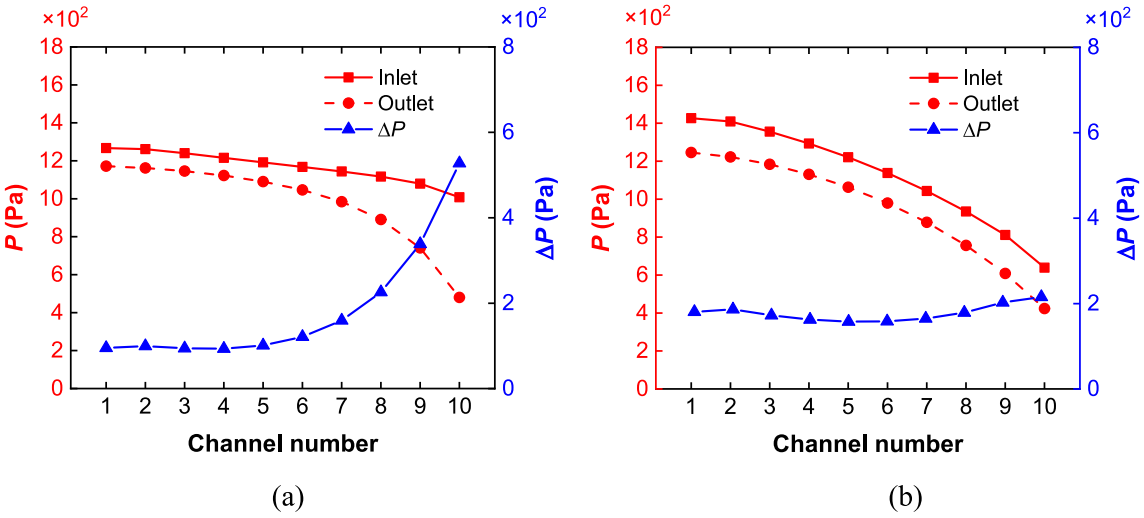

Fig. 10. Pressures of the parallel channels in the PMCHSs: (a) PMCHS-0, (b) PMCHS-opt2 ($\dot{m}_0$=1 g/s).

PMCHS-0. As the flow rate of the first channel in PMCHS-opt2 is larger than that in PMCHS-opt1, T_{max} of PMCHS-opt2 is lower. Moreover, the increase of inlet deflector angle decreases the divergence channel width, thus increases the drag of the water. The pumping power of PMCHS-opt2 (0.00123 W) is increased by 22% compared with PMCHS-0 (0.00101 W). In spite of this, by optimizing the inlet deflector angle using the FRN model, the cooling performance of the PMCHS can be significantly improved.

5.3.2. Optimization of the curved deflector

The results in Section 5.3.1 show that by optimizing the inlet deflector angle, the flow rate distribution of the parallel channels can be homogenized and the cooling performance of the PMCHS can be improved significantly. In this section, the curved deflector is considered and the FRN model is adopted to optimize the shape of the inlet deflector for improvement of the performance of PMCHSs. The width distribution $\mathbf{W_{DC}}$ is introduced to describe the local widths of the divergence channel (as shown in Fig. 11), which can be used to describe the shape of the inlet deflector. Thus, $\mathbf{W_{DC}}$ can be defined as follows:

$$\mathbf{W_{DC}} = [w_{DC,1}, \cdots, w_{DC,i}, \cdots, w_{DC,N-1}] \tag{32}$$

where $w_{DC,i}$ is the channel width of the i-th segment of the divergence channel.

Similar to the investigation in Section 5.2, based on the FRN model, the optimization of $\mathbf{W_{DC}}$ in PMCHSs can be transformed into a simpler process of searching the optimal flow rates among micro-channels. When the flow rates of parallel channels are given, $\mathbf{W_{DC}}$ can be calculated by solving the FRN model. In this situation, the unknown variables are $U_{PC,i}$, $U_{CC,i}$, $U_{DC,i}$ and $w_{DC,i}$, with a total number of $(4N-1)$. The FRN model in Eq. (9), Eqs. (22)–(24) gives $(4N-1)$ equations. Therefore, the width distribution of divergence channels $\mathbf{W_{DC}}$ can be directly solved using the FRN model.

Considering the PMCHS in Section 2, the inlet flow rate $\dot{m}_0$ is 1 g/s, the widths of parallel channels are set as identical at 1 mm, and the widths of the convergence channel are set as identical at 3 mm. The optimal flow rate distribution $\dot{\mathbf{m}}_{PC}$ is set to a uniform distribution. By using the FRN model, the optimized width distribution $\mathbf{W_{DC,opt}}$ can be calculated, with the results shown as:

$$\mathbf{W_{DC,opt}} = [2.85, 2.60, 2.26, 1.87, 1.47, 1.11, 0.79, 0.52, 0.29] \text{ mm} \tag{33}$$

The PMCHS with optimization of the curved deflector denoted as PMCHS-opt3. It can be seen that, from the inlet to the outlet, the optimized widths of the divergence channel gradually decrease in the order. Similar to the optimization of the inlet deflector angle, the reduction of the divergence channel width will reduce the pressure loss of the parallel channels far from the inlet, leading to reduction of the water going through the corresponding parallel channels. Thus, the optimized $\mathbf{W_{DC}}$ expressed as Eq. (33) is beneficial for increase of the flow rates of parallel channels near the inlet and decrease those near the outlet, which

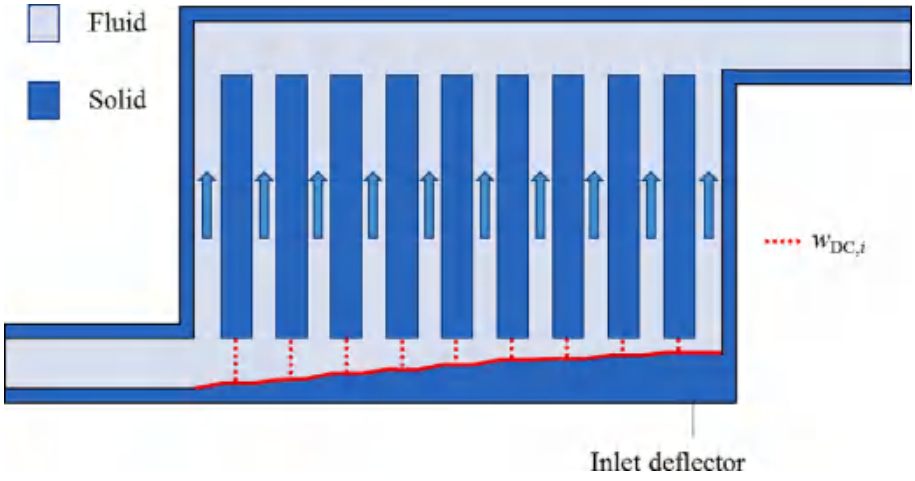

Fig. 11. Schematic diagram of the curved inlet deflector.

can effectively homogenize the flow rates among parallel channels. Fig. 5d shows the flow contour of PMCHS-opt3. Similar to PMCHS-opt2, optimization of inlet deflector shape results in the decreased widths for the divergence channel from the inlet to the outlet, which effectively improves the flow rate distribution. Fig. 12 depicts the flow rates of parallel channels in PMCHS-opt3 calculated using the CFD method, which shows a significant reduced flow rate difference. The flow rates of PMCHS-opt3 are all around 0.1 g/s, which is similar to the set uniform flow rate distribution. The widths of the divergence channel corresponding to the given flow rate distribution can be effectively calculated by the FRN model. Compared with that in PMCHS-0, the homogenization of the flow rates of parallel channels in PMCHS-opt3 is improved effectively, with $\sigma_{\dot{m}}$ at 0.0079, which is reduced by 87%. The more uniform distribution of flow rate thus ensures a more uniform distribution of temperature, with the hot spot temperature reduced and the temperature uniformity of heating surface remarkably improved (Table 4). Compared with those in PMCHS-0, $T_{\max}$ and σ_T in PMCHS-opt3 decrease by 4.8 K and 14% respectively. The pumping power of PMCHS-opt3 is similar to PMCHS-opt2, which is increased by 24% compared with PMCHS-0.

Furthermore, the position of the hot spot temperature in PMCHS-opt3 is not located at the downstream of the first parallel channel, but at the downstream of Channel #8, which is different from PMCHS-opt1 and PMCHS-opt2. This is because the flow rates of the channels around the inlet (Channel #1–#6) are larger than 0.1 g/s and those around the outlet (Channel #7–#10) are smaller than 0.1 g/s in PMCHS-opt3. The smaller flow rates around Channel #8 result in the hot spot. In spite of this, $T_{\max}$ of PMCHS-opt3 is lower than those of PMCHS-opt1 and PMCHS-opt2. Therefore, by optimizing the shape of the inlet deflector using the FRN model, the cooling performance of the PMCHS can be effectively improved.

6. Conclusion

In this study, an FRN model is established to enable the effective structural optimization of three-dimensional PMCHSs. The coefficient related to the channel shape for calculation of friction pressure loss in three-dimensional micro-channel is suggested. The results show that the flow rate distribution obtained by the FRN model agrees well with the CFD results. The developed model establishes the relationship between the structural parameters of PMCHSs and the flow rate distribution in parallel channels. The optimizations of parallel channel widths and deflector shape are carried out by adopting equal flow rates in parallel channels and using the FRN model. The results indicate that the flow rate distribution among parallel channels is effectively homogenized after the optimization for both systems, which ensures enhanced cooling performance. Compared with the PMCHS before optimization, $T_{\max}$ and σ_T of the PMCHS with optimized channel widths decrease by 4.0 K and 20%, respectively. Further analysis shows that the shape of the inlet deflector significantly influences the cooling performance of PMCHSs, and the system with the curved deflector performs better than the linear one in PMCHSs. Compared with the PMCHS before optimization, $T_{\max}$ and σ_T in the PMCHS with optimized inlet deflector shape decrease by 4.8 K and 14%, respectively. The FRN model is a general model, and can be used for three-dimensional PMCHSs with different structural parameters and operating parameters. Thus, the developed optimization method based on the FRN model is applicable for structural design of PMCHSs with different structural parameters and operating conditions. The developed method facilitates the energy saving and reliability enhancement of electronics especially when they serve at critical environment.

Declaration of Competing Interest

The authors declare that they have no known competing financial interests or personal relationships that could have appeared to influence the work reported in this paper.

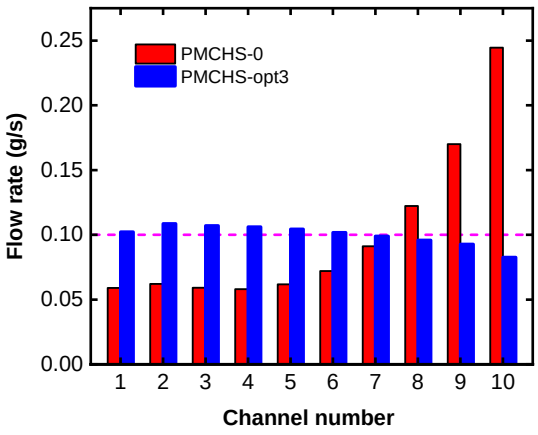

Fig. 12. Flow rates of the PMCHSs in PMCHS-0 and PMCHS-opt3.

Data availability

Data will be made available on request.

Acknowledgements

This research is supported by National Natural Science Foundation of China (Grant Nos. 51976062 and 52006050), the Fundamental Research Funds for the Provincial Universities of Zhejiang (Grant No. GK219909299001-005), Science and Technology Program of Guangzhou (Grant No. 202102020563). The authors acknowledge the Beijing Super Cloud Center (BSCC) for providing HPC resources that have contributed to the research results reported within this paper.URL: http://www.blsc.cn/

References

[1] X. Chen, T. Ding, H. Cao, H. Ding, Z. Li, Flow boiling heat transfer mechanisms and flow characteristics of pump-driven two-phase flow systems used in data center cooling br, Appl. Therm. Eng. 220 (2023), 119642.
[2] X. Wang, H. Li, R. Yao, W. Lai, R. Liu, R. Yu, X. Chen, J. Li, Thermal contact resistance optimization of press-pack IGBT device based on liquid metal thermal interface material, IEEE Trans. Power Electron. 37 (5) (2022) 5411–5420.
[3] U. Mustafa, I. Qeays, M. Binarif, S. Yahya, S. Ayob, Efficiency improvement of the solar PV-system using nanofluid and developed inverter topology, Energy Sources Part A 3 (2020) 1–17.
[4] J. Zhang, X. Wu, D. Zhou, Q. Li, X. Li, K. Chen, Experimental and numerical investigation on efficient optimization of battery thermal management systems, Appl. Therm. Eng. 221 (2023), 119821.
[5] L. Nakharintr, P. Naphon, S. Wiriyasart, Effect of jet-plate spacing to jet diameter ratios on nanofluids heat transfer in a mini-channel heat sink, Int. J. Heat Mass Transf. 116 (2018) 352–361.
[6] H. Ahmed, B. Salman, A. Kherbeet, M. Ahmed, Optimization of thermal design of heat sinks: A review, Int. J. Heat Mass Transf. 118 (2018) 129–153.
[7] G. Lee, S. Kim, Thermal optimization of radial plate fin heat sinks under an L-shaped flow, Appl. Therm. Eng. 133 (2018) 580–587.
[8] A. Zou, R. Chuan, F. Qian, W. Zhang, Q. Wang, C. Zhao, Topology optimization for a water-cooled heat sink in micro-electronics based on Pareto frontier, Appl. Therm. Eng. 207 (2022), 118128.
[9] G. Hetsroni, A. Mosyak, E. Pogrebnyak, Z. Segal, Periodic boiling in parallel microchannels at low vapor quality, Int. J. Multiph. Flow 32 (10–11) (2006) 1141–1159.
[10] P. Wang, A. Bar-Cohen, On-chip hot spot cooling using silicon thermoelectric microcoolers, J. Appl. Phys. 102 (3) (2007) 34503.
[11] S. Wiriyasart, P. Naphon, Heat spreading of liquid jet impingement cooling of cold plate heat sink with different fin shapes, Case Stud. Therm. Eng. 20 (2020), 100638.
[12] X. Cao, H. Liu, X. Shao, H. Shen, G. Xie, Thermal performance of double serpentine minichannel heat sinks: Effects of inlet-outlet arrangements and through-holes, Int. J. Heat Mass Transf. 153 (2020), 119575.
[13] L. Xu, Y. Xu, H. Gu, S. Qiu, A. Mujumdar, P. Xu, Thermal-hydraulic performance of flat-plate microchannel with fractal tree-like structure and self-affine rough wall, Eng. Appl. Comput. Fluid Mech. 17 (1) (2023) 2153174.

[14] L. Gong, J. Zhao, S. Huang, Numerical study on layout of micro-channel heat sink for thermal management of electronic devices, Appl. Therm. Eng. 88 (2015) 480–490.
[15] H. Wang, Q. Wu, C. Wang, R. Wang, A universal high-efficiency cooling structure for high-power integrated circuits, Appl. Therm. Eng. 215 (2022), 118849.
[16] R. Kumar, G. Singh, D. Mikielewicz, A new approach for the mitigating of flow maldistribution in parallel microchannel heat sink, J. Heat Transfer 140 (7) (2018), 072401.
[17] G. Xie, Y. Li, F. Zhang, B. Sunden, Analysis of micro-channel heat sinks with rectangular-shaped flow obstructions, Numer. Heat Transf. Part A, Appl. 69 (4) (2016) 335–351.
[18] S. Kim, I. Mudawar, Analytical heat diffusion models for different micro-channel heat sink cross-sectional geometries, Int. J. Heat Mass Transf. 53 (19–20) (2010) 4002–4016.
[19] Z. Wang, X. Wang, W. Yan, Y. Duan, D. Lee, J. Xu, Multi-parameters optimization for microchannel heat sink using inverse problem method, Int. J. Heat Mass Transf. 54 (13–14) (2011) 2811–2819.
[20] D. Lin, C. Kang, S. Chen, Optimization of the micro channel heat sink by combing genetic algorithm with the finite element method, Inventions 3 (2) (2018) 32.
[21] A. Yildizeli, S. Cadirci, Multi objective optimization of a micro-channel heat sink through genetic algorithm, Int. J. Heat Mass Transf. 146 (2020), 118847.
[22] H. Wang, X. Chen, Numerical simulation of heat transfer and flow of Al2O3-water nanofluid in microchannel heat sink with cantor fractal structure based on genetic algorithm, Anal. Chim. Acta 1221 (2022), 339927.
[23] H.A. Kose, A. Yildizeli, S. Cadirci, Parametric study and optimization of microchannel heat sinks with various shapes, Appl. Therm. Eng. 211 (2022), 118368.
[24] X. Shang, Q. Li, Q. Cao, Z. Li, W. Shao, Z. Cui, Mathematical modeling and multi-objective optimization on the rectangular micro-channel heat sink, Int. J. Therm. Sci. 184 (2023), 107926.
[25] L. Kwanda, Multi-objective optimization of a rectangular micro-channel heat sink using the augmented ε-constraint method, Eng. Optim. 52 (1) (2020) 22–36.
[26] C. Amador, A. Gavriilidis, P. Angeli, Flow distribution in different microreactor scale-out geometries and the effect of manufacturing tolerances and channel blockage, Chem. Eng. J. 101 (1–3) (2004) 379–390.
[27] C. Li, P. Huang, M. Pan, Reverse optimization algorithm of velocity uniformity in microchannels based on a simplified resistance network model, Chem. Eng. Sci. 221 (2020), 115655.
[28] K. Chen, D. Zhou, X. Wu, J. Zhang, M. Song, A novel optimization method based on inverse calculation model for efficient design of battery thermal management system, Energ. Conver. Manage. 255 (2022), 115290.
[29] R. Shah, A. London, Laminar Flow Forced Convection in Ducts, Academic Press, New York, 1978, pp. 224–246.
[30] Z. Liu, Y. Wang, J. Zhang, Z. Liu, Shortcut computation for the thermal management of a large air-cooled battery pack, Appl. Therm. Eng. 66 (1–2) (2014) 445–452.
[31] J. Zhang, X. Wu, K. Chen, D. Zhou, M. Song, Experimental and numerical studies on an efficient transient heat transfer model for air-cooled battery thermal management systems, J. Power Sources 490 (2021), 229539.
[32] M. Bassett, D. Winterbone, R. Pearson, Calculation of steady flow pressure loss coefficients for pipe junctions, Proc. Inst. Mech. Eng. C J. Mech. Eng. Sci. 215 (8) (2001) 861–881.
[33] J. Hou, X. Wu, K. Chen, Y. Dong, A direct optimization strategy based on field synergy equation for efficient design of battery thermal management system, Int. J. Heat Mass Transf. 184 (2022), 122304.